catalysts

MDPI

Article

CuO Nanoparticles Supported on TiO_2 with High Efficiency for CO_2 Electrochemical Reduction to Ethanol

Jing Yuan, Jing-Jie Zhang, Man-Ping Yang, Wang-Jun Meng, Huan Wang * and Jia-Xing Lu *

Shanghai Key Laboratory of Green Chemistry and Chemical Processes, School of Chemistry and Molecular Engineering, East China Normal University, Shanghai 200062, China; yuanjing158yj@126.com (J.Y.); zjj18221019582@163.com (J.-J.Z.); YMP2018@126.com (M.-P.Y.); mwjynl@outlook.com (W.-J.M.)

* Correspondence: hwang@chem.ecnu.edu.cn (H.W.); jxlu@chem.ecnu.edu.cn (J.-X.L.); Tel.: +86-21-5213-4935 (H.W.); +86-21-6223-3491 (J.-X.L.)

Received: 7 March 2018; Accepted: 18 April 2018; Published: 21 April 2018

Abstract: Non-noble metal oxides consisting of CuO and TiO_2 (CuO/TiO_2 catalyst) for CO_2 reduction were fabricated using a simple hydrothermal method. The designed catalysts of CuO could be in situ reduced to a metallic Cu-forming Cu/TiO_2 catalyst, which could efficiently catalyze CO_2 reduction to multi-carbon oxygenates (ethanol, acetone, and n-propanol) with a maximum overall faradaic efficiency of 47.4% at a potential of −0.85 V vs. reversible hydrogen electrode (RHE) in 0.5 M $KHCO_3$ solution. The catalytic activity for CO_2 electroreduction strongly depends on the CuO contents of the catalysts as-prepared, resulting in different electrochemistry surface areas. The significantly improved CO_2 catalytic activity of CuO/TiO_2 might be due to the strong CO_2 adsorption ability.

Keywords: electrochemical reduction; CO_2; CuO; TiO_2; ethanol

1. Introduction

Electrochemical reduction of CO_2 (CO_2ER) is a promising and feasible method with which to sustainably transform this waste stream into value-added low-carbon fuels [1–5], which has the following advantages: (1) An electrochemical system can be operated under moderate reaction conditions [5,6]; (2) The reaction process involves highly complex multiple protons and electrons transfer steps, which lead to wide product distribution, such as methanol, ethanol, acetone, and so on [7,8]; (3) The electricity could be supplied by clean and sustainable energy, such as solar, wind, and hydropower [9,10]; and (4) This reaction requires minimal chemical intake and is convenient for large-scale applications [5,8]. However, CO_2ER is facing severe challenges, including poor faradaic efficiency (FE), high overpotential, and low selectivity [11,12], which urges us to design new catalysts to address the above efficiency and selectivity issues.

Over the past few decades, numerous trials have been made to explore catalysts with distinguished performance for CO_2ER. Until now, multifarious catalysts including metals [5,11–13], metal oxides [14–16], and metal complexes [17,18] have been reported. Among these catalysts, Cu, as a relatively low-cost and earth abundant metal, has a unique capacity to produce hydrocarbons through a multiple protons and electrons transfer pathway; however, the traditional Cu catalysts show high overpotential [16] and low selectivity for diversiform products [5,12,19–21]. Substantial efforts have been pursued to enhance energetic efficiency for CO_2ER through altering surface structures, morphologies, and the nature compositions. Recently, Cu-based catalysts have been reported to possess enhanced FEs for CO_2ER; for instance, Takanabe et al. [22] used Cu-Sn alloy for the efficient and selective reduction of CO_2 to CO over a wide potential range. Yu and her team [23] reported that Cu nanoparticle (NP) interspersed MoS_2 nanoflowers facilitate CO_2ER to hydrocarbon, such as

CH_4 and C_2H_4 with high FE at low overpotentials. Sun et al. [24] introduced a Core/Shell Cu/SnO_2 structure that shows high selectivity to generate CO with FE reaching 93% at −0.7 V (vs. the reversible hydrogen electrode (RHE)).

Normally, TiO_2, as a semiconductor material, is one of the most widely used photocatalysts and electrocatalysts for CO_2 reduction because of its nontoxicity, low cost, and high chemical stability [25,26]. Furthermore, TiO_2 has been reported to act as a redox electron carrier to facilitate a variety of reduction reactions, including CO_2 conversion [27,28], and to assist in CO_2 adsorption [29,30]; thus, it may stabilize the CO_2ER intermediate and reduce overpotential. Some early works could verify this point in the CO_2ER, such as Ag/TiO_2 [31], Cu/TiO_2 [32], and Cu/TiO_2/N-graphene [33].

CuO/TiO_2 has been previously prepared using different synthetic methods and is used for various applications, such as photodriven reduction of CO_2 [34] and hydrogen production reaction [35]. Nevertheless, to the author's knowledge, CuO/TiO_2 as electrocatalysts for CO_2ER have been rarely investigated. In previous works, we have demonstrated that CuO with various morphologies can be highly efficient electrocatalysts for CO_2 reduction to ethanol in simple aqueous medium, but at high overpotential (−1.7 V vs. the saturated calomel electrode (SCE)) [36]. Inspired by previous studies, in this work, we systematically and carefully synthesized a series of nano-sized CuO/TiO_2 catalysts for CO_2ER. The prepared CuO/TiO_2 catalysts were optimized by varying the amount of loaded CuO NPs. CuO/TiO_2 with an intended CuO content of 60%, as an efficient electrocatalyst, exhibits the most outstanding activity (achieved total FE of 47.4% at the potential of −0.85 V vs. RHE) for CO_2ER in 0.5 M $KHCO_3$ solution at room temperature among all as-prepared CuO/TiO_2 catalysts.

2. Results and Discussion

2.1. Catalyst Characterizations

A simple and mild hydrothermal synthesis method was used to prepare six different weight ratios of CuO/TiO_2 catalysts, which are defined as CuO/TiO_2-1, CuO/TiO_2-2, CuO/TiO_2-3, CuO/TiO_2-4, CuO/TiO_2-5, and CuO/TiO_2-6, corresponding to the intended CuO content of 5 wt %, 10 wt %, 20 wt %, 40 wt %, 60 wt %, and 80 wt %, respectively. X-ray diffractometer (XRD) patterns shown in Figure 1 indicated that these catalysts consist of both CuO and TiO_2, which were represented by solid lines and dashed lines, respectively. It can be clearly seen that all as-prepared catalysts with different amounts of CuO loadings present similar XRD patterns. The diffraction peaks ascribed to CuO were significantly shown with the increasing of CuO contents in the XRD patterns. Meanwhile, the actual CuO contents were analyzed by inductively coupled plasma atomic emission spectroscopy (ICP-AES) and summarized in Table S1. These values are in good agreement with the intended values.

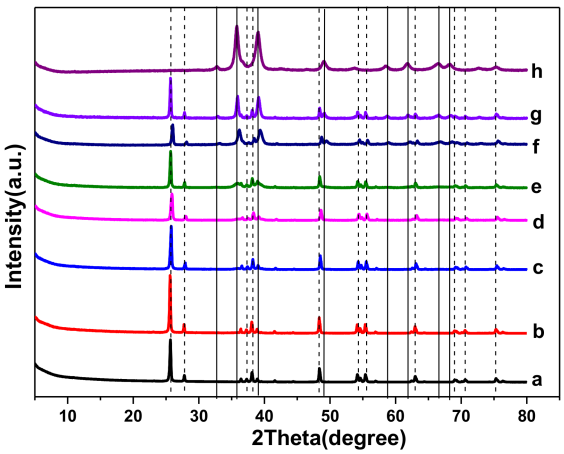

Figure 1. XRD patterns of (**a**) pure TiO_2, (**b**) CuO/TiO_2-1, (**c**) CuO/TiO_2-2, (**d**) CuO/TiO_2-3, (**e**) CuO/TiO_2-4, (**f**) CuO/TiO_2-5, (**g**) CuO/TiO_2-6, and (**h**) pure CuO.

To thoroughly examine the element proportion and chemical state of CuO/TiO_2 catalysts, X-ray photoelectron spectroscopy (XPS) of CuO/TiO_2-5 catalyst was investigated. As expected, Cu, Ti, and O elements from CuO/TiO_2 catalyst were observed in the full spectrum from Figure 2a. Furthermore, Figure 2b displays the high resolution spectrum of Cu 2p, separated into Cu $2p^{3/2}$ and Cu $2p^{1/2}$ at 933.8 eV and 953.8 eV, respectively. The distance between these Cu 2p main peaks positions is 20.0 eV, which agrees well with previous reports about CuO spectrum [37]. Moreover, additional confirmation of CuO state was seen with the broad satellite peaks at a higher binding energy than the main peaks. The main peak of Cu $2p^{3/2}$ at 933.8 eV was accompanied by two satellite peaks on the higher binding energy side at about 943.8 eV and 941.5 eV, which suggests the existence of CuO [38–41]. From this figure, we can clearly see that the main peak of Cu $2p^{1/2}$ at 953.8 eV and its satellite peak at 962.5 eV were separated by about 9.0 eV, which also confirms the presence of CuO [42]. Both Ti $2p^{3/2}$ and Ti $2p^{1/2}$ peaks at 458.7 eV and 464.4 eV, respectively, were observed (Figure 2c) with a separation of 5.7 eV, indicating that TiO_2 existed in this catalyst [43]. The obtained XPS spectrum of O 1 s was presented in Figure 2d. An obvious peak appeared at 529.7 eV, which can be indexed to O^{2-} in the CuO and TiO_2. Notably, there are other three weak O 1 s peaks. One located at 530.7 eV is identified with surface hydroxyls, which is likely the by-product from the synthesis process of CuO/TiO_2. Additionally, the remaining two peaks observed at 531.5 eV and 532.8 eV are confirmed to C=O and C-O [44,45]. A slight peak of C 1 s was detected in Figure 2a, which is always observed in XPS spectra of real-world solids [46,47]. The high resolution spectrum of C 1 s was shown in Figure S1, consistent with the results of O 1 s.

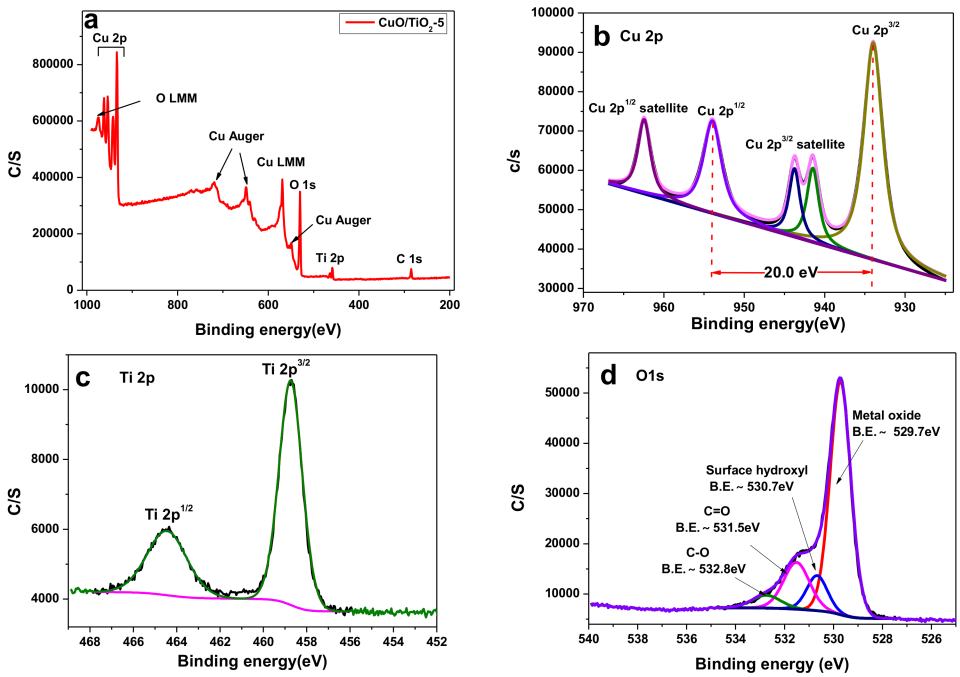

Figure 2. (**a**) The full XPS spectrum of CuO/TiO_2-5 catalyst and high-resolution XPS spectra of (**b**) Cu 2p; (**c**) Ti 2p and (**d**) O 1 s.

To obtain the morphological information regarding the CuO/TiO_2 catalysts, scanning electron microscope (SEM) images were firstly shown in Figure S2. One can see that the catalysts were composed of 3-dimension NPs with a certain amount of CuO nano-floc supported on the surface of TiO_2. Further from the SEM images, for low CuO content of CuO/TiO_2 (5 wt %, 10 wt %, and 20 wt %), CuO NPs were dotted sporadically on the surface of TiO_2. Subsequently, for high CuO content of CuO/TiO_2 (40 wt %, 60 wt %, and 80 wt %), it is evident that the CuO NPs completely covered on the TiO_2 surface forming a massive and compact layer. Pure CuO NPs presented very

porous, sponge-like structures. Moreover, transmission electron microscopy (TEM) investigation was used to gain deeper insight into the structural feature of the catalysts. TEM of CuO/TiO_2-5 was shown in Figure 3a. Numerous CuO NPs were irregularly interspersed on the TiO_2 surface, in accordance with the SEM results. High-resolution TEM images of CuO/TiO_2-5 were displayed in Figure 3b to acquire more detailed information about the structure of the catalyst. The fast Fourier transform (FFT, inset of Figure 3b) pattern of CuO and TiO_2 shows concentric rings and bright discrete diffraction spots, which are indicative of high crystallinity. From Figure 3b, distinctive lattice fringes were found in both TiO_2 and CuO NPs. The lattice fringes with interplanar spacing of 0.188 nm were assigned to the (200) plane of the TiO_2, expressed by orange lines (inserted in Figure 3b). Additionally, the lattice fringes with d-spacings of 0.256 nm corresponded to the plane (111) of CuO phase, represented by the yellow lines (inserted in Figure 3b).

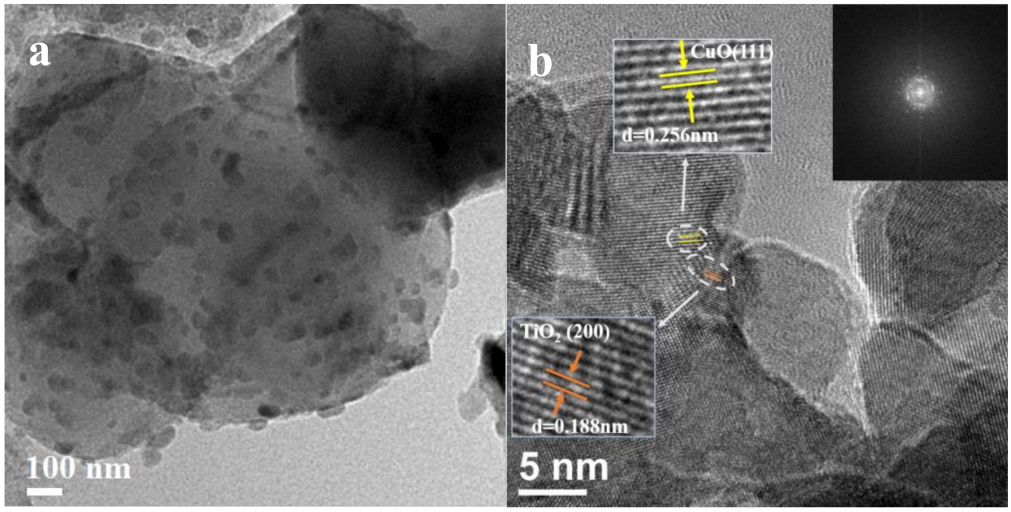

Figure 3. TEM images of CuO/TiO_2-5 catalyst in (**a**) low magnification and (**b**) high magnification (the insets are FFT pattern and the detailed images of white dashed circle).

2.2. Catalyst Properties

The electrocatalytic activity of CuO/TiO_2-5 catalyst was carried out in the typical three-electrode system through cyclic voltammetry (CV) measurement, which was firstly tested at a scan rate of 50 mV/s in N_2-saturated and CO_2-saturated 0.5 M $KHCO_3$ solution, respectively, as shown in Figure 4a. In both N_2 and CO_2 atmosphere, two obvious reduction peaks were observed, corresponding to the in situ reduction of CuO to Cu_2O and sequentially Cu_2O to Cu [48]. As expected, XRD characterization could verify the formation of Cu metal from CuO/TiO_2-5 catalyst after 2 h electrolysis, depicted in Figure S3. Three significant diffraction peaks for metallic Cu (denoted by solid diamond) appeared, suggesting that CuO NPs in CuO/TiO_2-5 catalyst could be in situ electroreduced to metallic Cu-forming Cu/TiO_2 in the electrolysis process and subsequently serves as an effective catalyst for CO_2 reduction, verified by previous reports [16,36,47]. In the more negative potential region, an obvious increase of current density (J) after −0.65 V vs. RHE was shown, relating to the hydrogen evolution reaction (HER) in the N_2-saturated 0.5 M $KHCO_3$ solution (pH = 8.63, black line), while more dramatic increase of J was observed in the CO_2-saturated 0.5 M $KHCO_3$ solution (pH = 7.21, red line). To avoid the pH effect, a CV curve was recorded in the N_2-saturated solution with HCl solution (pH = 7.21, same as that of the CO_2-saturated 0.5 M $KHCO_3$ solution, blue line), which shows lower J than that in CO_2-saturated 0.5 M $KHCO_3$ solution after −0.65 V vs. RHE. It demonstrates that CO_2 reduction is more favorable than HER on CuO/TiO_2-5.

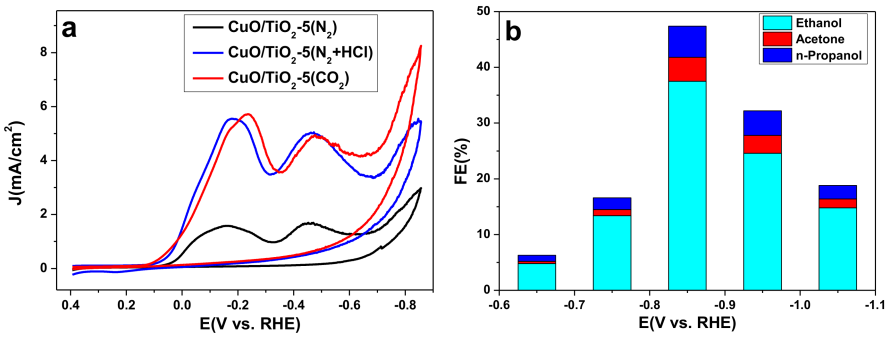

Figure 4. (**a**) CV curves of CuO/TiO_2-5 catalyst over glassy carbon electrode (GCE) in N_2-saturated without (black line) and with (blue line) HCl solution, and CO_2-saturated (red line) 0.5 M $KHCO_3$ solution; (**b**) FEs for different products over CuO/TiO_2-5 catalyst at various potentials.

The CO_2ER electrocatalytic activity on CuO/TiO_2-5 catalyst was also evaluated by controlled potential electrolysis (from −0.65 V to −1.05 V vs. RHE) in CO_2-saturated 0.5 M $KHCO_3$ solution. The main liquid products of the electrolysis are ethanol, acetone, and n-propanol, which were detected by ^{1}H NMR. The overall FEs (Figure 4b) presented a sharply incremental tendency at an applied potential range from −0.65 V to −0.85 V vs. RHE and achieved a maximum of 47.4% (37.5% for ethanol, 4.3% for acetone, and 5.6% for n-propanol) at the potential of −0.85 V vs. RHE. As the potentials shift more negatively, the overall FEs significantly decreased to 18.8% at the potential of −1.05 V vs. RHE because of the competition from HER. Furthermore, a similar variation trend for $FE_{ethanol}$, $FE_{acetone}$, and $FE_{n\text{-propanol}}$ was observed and depicted in detail in Figure 4b. Moreover, Figure S4 shows the total current vs. time curve for the CuO/TiO_2-5 electrode at −0.85 V vs. RHE, which exhibited an initial current of 85 mA as the CuO was reduced and, subsequently, a sharp decline current in a short time. Finally, a stable current of 16 mA in the long test appeared. Notably, the FE for ethanol was maintained at approximately 35% throughout the electrolysis. This finding suggests not only efficient but also stable activity for CO_2 reduction on this electrode.

We also studied the effect of CuO contents in various CuO/TiO_2 catalysts on CO_2ER activities, as shown in Figure 5a. All CuO/TiO_2 catalysts showed two obvious reduction peaks in the CO_2-saturated 0.5 M $KHCO_3$ solution; however, the position and size of the reduction peaks varied greatly among the catalysts, which, assigned to in situ, reduce CuO to Cu. Noteworthily, in the more negative potential region (below −0.65 V vs. RHE), all CuO/TiO_2 catalysts show different catalytic abilities for CO_2 reduction. The J of all CuO/TiO_2 catalysts at a potential of −0.85 V vs. RHE were summarized in Table S2. CuO/TiO_2-5 showed the largest J. The dramatic difference of electrocatalytic performance on various CuO/TiO_2 catalysts might be closely related to the composition of these catalysts. Figure 5a shows that increasing the CuO content (from 5 wt % to 60 wt %) in the CuO/TiO_2 catalysts can facilitate the reduction of CO_2, leading to enhanced activity for CO_2 reduction. However, on the CuO/TiO_2-6 (with the intended CuO content of 80 wt %) catalyst for sequentially increasing the content of CuO, CO_2 reduction was subsequently suppressed. The results clearly indicate that an optimum content of CuO in the catalysts is required to achieve the maximum activity for CO_2 reduction.

Potentiostatic electrolysis (at −0.85 V vs. RHE) of CO_2 on various CuO/TiO_2 catalysts was performed in CO_2-saturated 0.5 M $KHCO_3$ solution to further investigate the catalytic activities of CuO/TiO_2 catalysts with different CuO contents. Figure 5b summarizes the FEs of ethanol, acetone, and n-propanol achieved over all CuO/TiO_2 catalysts. As expected, the CuO/TiO_2-5 with the intended CuO content of 60 wt % gives the highest total FE, which reached 47.4%, when compared with other CuO/TiO_2 catalysts, which is in a well agreement with CV results as shown in Figure 5a. However, the total FEs decreased along with the higher CuO content (80 wt % and even 100 wt %) of CuO/TiO_2, which is ascribed to the large number of CuO NPs that accumulated on the surface of TiO_2, as shown in Figure S2f,g, which probably generated the decrease of active areas for CO_2ER. Yet, low CuO

content (5 wt %–40 wt %) of CuO/TiO_2 also exhibited slightly poor electrocatalytic performance for CO_2ER due to the low content of CuO NPs. It demonstrates further that the catalytic activity for CO_2ER strongly depends on the CuO contents of the catalysts as-prepared, which results in different electrochemistry surface areas (ECSA). To confirm this finding, ECSA of a variety of CuO/TiO_2 electrodes were examined by CV in a potential range in which the faradaic process did not occur with the double layer capacitance in N_2 atmosphere 0.1 M $HClO_4$ solution (Figure S5 and Table S3). As expected, CuO/TiO_2-5 catalyst showed a noticeable performance improvement for the double layer capacitance (C_{dl}), which gives the positive correlation with ECSA. The C_{dl} in Table S3 indicated the ECSA increased with increasing CuO content up to 60 wt %; however, a slight decrease was observed at 80 wt %, which reconfirms the CuO content of CuO/TiO_2 catalysts plays a vital role in ECSA that can affect CO_2ER, which is in accordance with the results of Brunauer− Emmett−Teller (BET) specific surface area (Table S4).

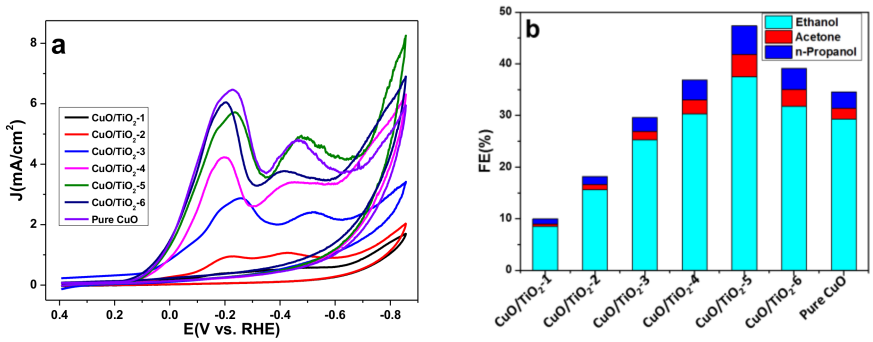

Figure 5. (**a**) CV curves of various CuO/TiO_2 catalysts over GCE in CO_2-saturated 0.5 M $KHCO_3$ solution. Scan rate, 50 mV/s; (**b**) FEs for different products over various CuO/TiO_2 catalysts at −0.85 V vs. RHE in CO_2-saturated 0.5 M $KHCO_3$ aqueous solution.

To further study the improved performance of CuO/TiO_2-5 catalyst, we compared the electrocatalytic abilities of CO_2 reduction on CuO/TiO_2-5 and CuO/C catalysts. The CuO/C was successfully synthesized and characterized by XRD (Figure S6), SEM, and TEM (Figure S7). CuO/C catalyst represents the onset potential for CO_2 reduction at −0.75 V vs. RHE, corresponding to a 0.10 V more negative onset potential than CuO/TiO_2-5, as shown in Figure S8. This finding suggests that TiO_2 as the supporter is more beneficial to facilitating CO_2ER. The J in CO_2-saturated solution of CuO/TiO_2-5 at the potential of −0.85 V vs. RHE was 8.307 mA/cm^2, which is larger than that of CuO/C (1.402 mA/cm^2). Additionally, potentiostatic electrolysis in CO_2-saturated 0.5 M $KHCO_3$ solution for the CuO/C was performed at the potential of −0.85 V vs. RHE, which shows poor active towards CO_2 reduction. Only 16.3% for overall FE (12.9% for ethanol, 1.1% for acetone, and 2.3% for n-propanol) was analyzed by ^{1}H NMR. In contrast, CuO/TiO_2-5 catalyst presents excellent activity for CO_2 reduction, which achieved 47.4% for overall FE. Besides, as seen from Figure S5 and Table S3, the ECSA of CuO/TiO_2-5 reveals a larger value than the one of CuO/C. As is well known, CO_2 adsorption on the active sites is the prerequisite for subsequent CO_2 reduction reaction. The relatively larger amount of CO_2 adsorption on active sites may offer more original reactants such as CO_2 [49]. The CO_2 adsorption abilities of CuO/TiO_2-5 and CuO/C were evaluated by CO_2 adsorption, which were displayed in Figure S9. CuO/TiO_2-5 catalyst possessed a more remarkably improved CO_2 adsorption capacity than CuO/C, which was 5.80 mg/g and 1.34 mg/g, respectively. It is reasonable to assume that the enhanced CO_2 adsorption capacity can make a significant contribution to the superior performance of CO_2 reduction. By comparing the electrochemical and material characterizations of CuO/TiO_2 with those of CuO/C, we gained insight that TiO_2 plays an important role in promoting the electrocatalytic performance of CuO/TiO_2. Hence, on the basis of the above analysis, a brief illustration of CO_2ER over CuO/TiO_2 catalysts is stated. Large amount of CO_2 is first adsorbed

on TiO_2. CuO/TiO_2 catalysts could be in situ electroreduced to Cu/TiO_2 at less negative cathode potentials than the ones of CO_2ER. Then, the adsorbed CO_2 gets one electron from the achieved Cu/TiO_2 electrode and is converted to CO_2^-, which can be dimerized to $*C_2O_2^-$. Notably, the C-C bond-making step on the Cu surface is a key step for CO_2 reduction to ethanol and even the C3 product (acetone and n-propanol) [50]. Interestingly, the catalytic ability of CuO/TiO_2-5 at −0.85 V vs. RHE expresses more obvious performance than the one of 40 wt % Cu/TiO_2 (the optimal catalyst in X wt % Cu/TiO_2 system) at −1.45 V vs. RHE [34], which indicates that in situ electroreduced Cu NPs have greater activity to catalyze CO_2 reduction. The low-cost CuO/TiO_2 catalyst is an efficient alternative to expensive materials for the application of CO_2ER in industry.

3. Materials and Methods

3.1. Materials and Instruments

Cupric acetate monohydrate [$Cu(Ac)_2{\cdot}H_2O$, Analytical Reagent (AR) grade], ammonium carbonate [$(NH_4)_2CO_3$, AR grade], potassium bicarbonate [$KHCO_3$, AR grade], and titanium dioxide [TiO_2, AR grade] were purchased from Sinopharm Chemical Reagent Co. (SCR, Shanghai, China) with 99% purity and used as received. Nafion® 117 solution (5%) and Nafion® 117 membrane were obtained from Dupont (Wilmington, DE, USA). Carbon paper (CP, HCP010) and conductive carbon black (C, VXC72R) were purchased from Shanghai Hesen Electrical CO. (Shanghai, China).

Crystal-phase X-ray diffraction (XRD) patterns of CuO/TiO_2 catalysts were recorded using an Ultima IV X-ray powder diffractometer (Kurary, Tokyo, Japan) equipped with Cu Kα radiation (k = 1.5406 Å). The values for actual CuO loadings of the synthesized catalysts were determined on an inductively coupled plasma atomic emission spectroscopy (ICP-AES, IRIS Intrepid II XPS, Waltham, MA, USA). The scanning electron microscope (SEM) images of the catalysts were obtained using a Hitachi S-4800 field-emission scanning electron microscope (Tokyo, Japan). Transmission electron microscopy (TEM) patterns were recorded by TECNAI G_2F30 transmission electron microscope (Tokyo, Japan). The X-ray photoelectron spectroscopy (XPS, Thermo Fisher Scientific, Waltham, MA, USA) analysis was performed on the Thermo Scientific ESCA Lab 250Xi using 200 W monochromatic Al Kα radiation. The 500 μm X-ray spot was used. The base pressure in the analysis chamber was about 3×10^{-10} mbar. Typically, the hydrocarbon C1s line at 284.8 eV from adventitious carbon was used for energy referencing. Brunauer−Emmett−Teller (BET) specific surface area was characterized by nitrogen adsorption in a BELSORP-MAX instrument (MicrotracBEL, Tokyo, Japan) after outgassing the samples for 10 h under vacuum at 573 K. CO_2 adsorption was obtained in a BELSORP-MAX instrument (MicrotracBEL, Japan) under CO_2 atmosphere at 298 K. Potentiostatic electrolysis and cyclic voltammetry (CV) were performed using a CHI 660 C electrochemical station (Shanghai Chenhua Instrument Co. Ltd., Shanghai, China).

3.2. Materials Synthesis

A simple and mild hydrothermal synthesis method was used to prepare six different weight ratios of CuO/TiO_2 catalysts, which are defined as CuO/TiO_2-1, CuO/TiO_2-2, CuO/TiO_2-3, CuO/TiO_2-4, CuO/TiO_2-5, and CuO/TiO_2-6, corresponding to the CuO content of 5 wt %, 10 wt %, 20 wt %, 40 wt %, 60 wt %, and 80 wt %, respectively. Typically, due to similar fabrication procedure, for simplicity, CuO/TiO_2-5 acts as the specimen to illustrate the following experiment. The detailed synthesis procedure for CuO/TiO_2-5 is depicted as follows: 0.05 M of $Cu(Ac)_2$ aqueous solution (60 mL) was mixed with 127 mg of TiO_2. After stirring for several minutes, an appropriate amount of 0.05 M of $(NH_4)_2CO_3$ aqueous solution was added drop-wise with stirring to control the synthetic rate. Then, the mixture was stirred gently for 3 h at the ambient temperature. Subsequently, the above mixture was centrifuged, washed with distilled water, and stored in a vacuum oven with 60 °C for 4 h to dry the precipitate. Finally, the collected powder was transferred to a crucible, further maintaining at 220 °C for 3 h to obtain the final CuO/TiO_2 powder. Pure CuO catalyst was acquired by the same

method, without adding TiO_2. Additionally, CuO/C catalyst with the CuO content of 60 wt % got through the similar synthetic process, but with C replacing TiO_2.

3.3. Electrode Preparation and Electrochemical Test

Potentiostatic electrolysis was carried out in an H-type three-electrode cell with a piece of Nafion® 117 cation exchange membrane (H^+ form) as a separator. The working electrode was manufactured using the following route: 10 mg of CuO/TiO_2 catalyst was suspended in a mixture solution with 20 μL of 5 wt % Nafion® solution and 40 μL of distilled water. After sonification for 20 min, the mixture was spread on a porous CP (2 × 2 cm) by micropipette and then dried in air. The counter and reference electrodes were Pt sheet and SCE, respectively. A 0.5 M of $KHCO_3$ aqueous solution serves as electrolyte, which was saturated with CO_2 by bubbling for 30 min before the electrolysis experiment. CO_2 was bubbled continuously throughout overall experiment time. CV tests were measured in a single cell system using a standard three-electrode setup at 0.5 M $KHCO_3$ aqueous solution under CO_2 and N_2 atmosphere with a scan rate of 50 mV/s, respectively. In this system, 2 μL of the above prepared catalyst suspension was coated on glassy carbon electrode (GCE, diameter = 2 mm) playing as the working electrode, and a Pt mesh and an SCE acted as the counter electrode and the reference electrode, respectively. All potentials were based on RHE as reference potentials, and converted by the following equation:

$$E \text{ (vs. RHE)} = E \text{ (vs. SCE)} + 0.059 \times \text{pH} + 0.241.$$

3.4. Product Analysis

Liquid phase products were analyzed by ^{1}H-nuclear magnetic resonance (NMR) spectra recorded on an Ascend 400 (400 MHz, Bruker, Germany) spectrometer in D_2O with Me_4Si as an internal standard.

4. Conclusions

In this study, a simple synthesis strategy was employed to fabricate CuO/TiO_2 material. A series of characterizations has demonstrated that CuO NPs were uniformly distributed on the surface of TiO_2. Different CuO/TiO_2 catalysts displayed dramatically different electrocatalytic performance for CO_2ER, depending strongly on the CuO contents of the catalysts as-prepared. High FEs of CO_2 reduction products (ethanol, acetone, and n-propanol) reach up to 47.4% on CuO/TiO_2-5 at the potential of −0.85 V vs. RHE among all CuO/TiO_2 and CuO/C catalysts. The CO_2 adsorption ability test suggests that CuO/TiO_2-5 exhibits more superior CO_2 adsorption performance than CuO/C, indicating that CuO/TiO_2-5 is more beneficial to CO_2 reduction. The fact that the as-synthesized CuO/TiO_2 catalysts exhibit high activity for CO_2ER is attributed to the special roles of TiO_2 that show excellent CO_2 adsorption ability. Our work may provide some concepts for designing cheap and effective catalysts for highly efficient CO_2ER.

Supplementary Materials: The following are available online at http://www.mdpi.com/2073-4344/8/4/171/, Table S1: CuO composition of the synthesized CuO/TiO_2 catalysts. Figure S1: The high-resolution XPS spectrum of C1s for CuO/TiO_2-5 catalyst. Figure S2: SEM images of (a) pure TiO_2, (b) CuO/TiO_2-1, (c) CuO/TiO_2-2, (d) CuO/TiO_2-3, (e) CuO/TiO_2-4, (f) CuO/TiO_2-5, (g) CuO/TiO_2-6, and (h) pure CuO. Figure S3: XRD patterns of CuO/TiO_2-5 catalyst after 2 h electrolysis. The solid diamond represents the in situ generated Cu metal. Figure S4: CO_2 reduction electrolysis data at −0.85 V vs. RHE for CuO-TiO_2-5 catalyst. Table S2: The current density (J) for all the CuO/TiO_2 catalysts in CO_2-saturated environment at the potential of −0.85 V vs. RHE. Figure S5: Plot of I vs. potential of (A) CuO/TiO_2-1, (B) CuO/TiO_2-2, (C) CuO/TiO_2-3, (D) CuO/TiO_2-4, (E) CuO/TiO_2-5, (F) CuO/TiO_2-6, (G) pure CuO, and (H) CuO/C in N_2-saturated 0.1 M $HClO_4$ solution cycled between 0.35 and 0.55 V vs. SCE at scan rates in the range of 5–60 mV/s. Insets show plot of I_c vs. ν in which the linear regressions give capacitance information. Table S3: The analysis of C_{dl} of various CuO/TiO_2 and CuO/C catalysts. Table S4: The analysis of specific surface area of CuO/TiO_2 catalysts. Figure S6: XRD patterns of CuO/C and C catalysts. Figure S7: SEM (a) and TEM (b) images of CuO/C catalyst. Figure S8: CV curve of CuO/C catalyst over glassy carbon electrode in CO_2-saturated (red line) 0.5 M $KHCO_3$ solution. Figure S9: CO_2 adsorption-desorption isotherms at 297 K of CuO/TiO_2-5 (red square) and CuO/C (blue triangle). Filled and empty symbols represent adsorption and desorption, respectively.

Acknowledgments: We gratefully acknowledge the financial support from the National Natural Science Foundation of China (21673078, 21473060, 21773071).

Author Contributions: Jing Yuan and Jing-Jie Zhang conceived and designed the experiments; Jing Yuan and Wang-Jun Meng performed the experiments; Jing Yuan, Man-Ping Yang, and Huan Wang analyzed the data; Jing Yuan, Huan Wang, and Jia-Xing Lu wrote the paper.

Conflicts of Interest: The authors declare no conflict of interest.

References

1. Kumar, B.; Brian, J.P.; Atla, V.; Kumari, S.; Bertram, K.A.; White, R.T.; Spurgeon, J.M. New trends in the development of heterogeneous catalysts for electrochemical CO_2 reduction. *Catal. Today* **2016**, *270*, 19–30. [CrossRef]
2. Qiao, J.L.; Liu, Y.Y.; Hong, F.; Zhang, J.J. A review of catalysts for the electroreduction of carbon dioxide to produce low-carbon fuels. *Chem. Soc. Rev.* **2014**, *43*, 631–675. [CrossRef] [PubMed]
3. Costentin, C.; Robert, M.; Saveant, J.M. Catalysis of the electrochemical reduction of carbon dioxide. *Chem. Soc. Rev.* **2013**, *42*, 2423–2436. [CrossRef] [PubMed]
4. Jitaru, M.; Lowy, D.A.; Toma, M.; Toma, B.C.; Oniciu, L. Electrochemical reduction of carbon dioxide on flat metallic cathodes. *J. Appl. Electrochem.* **1997**, *27*, 875–889. [CrossRef]
5. Kumar, B.; Brian, J.P.; Atla, V.; Kumari, S.; Bertram, K.A.; White, R.T.; Spurgeon, J.M. Controlling the Product Syngas H_2:CO Ratio through Pulsed-Bias Electrochemical Reduction of CO_2 on Copper. *ACS Catal.* **2016**, *6*, 4739–4745. [CrossRef]
6. Kondratenko, E.V.; Mul, G.; Baltrusaitis, J.; Larrazabal, G.O.; Perez-Ramírez, J. Status and perspectives of CO_2 conversion into fuels and chemicals by catalytic, photocatalytic and electrocatalytic processes. *Energy Environ. Sci.* **2013**, *6*, 3112–3135. [CrossRef]
7. Reske, R.; Duca, M.; Oezaslan, M.; Schouten, K.J.P.; Koper, M.T.M.; Strasser, P. Controlling Catalytic Selectivities during CO_2 Electroreduction on Thin Cu Metal Overlayers. *J. Phys. Chem. Lett.* **2013**, *4*, 2410–2413. [CrossRef]
8. Zhao, K.; Liu, Y.M.; Quan, X.; Chen, S.; Yu, H.T. CO_2 Electroreduction at Low Overpotential on Oxide-Derived Cu/Carbons Fabricated from Metal Organic Framework. *ACS Appl. Mater. Interfaces* **2017**, *9*, 5302–5311. [CrossRef] [PubMed]
9. Ohya, S.; Kaneco, S.; Katsumata, H.; Suzuki, T.; Ohta, K. Electrochemical reduction of CO_2 in methanol with aid of CuO and Cu_2O. *Catal. Today* **2009**, *148*, 329–334. [CrossRef]
10. Kaneco, S.; Iiba, K.; Katsumata, H.; Suzuki, T.; Ohta, K. Electrochemical reduction of high pressure carbon dioxide at a Cu electrode in cold methanol with CsOH supporting salt. *Chem. Eng. J.* **2007**, *128*, 47–50. [CrossRef]
11. Whipple, D.T.; Kenis, P.J.A. Prospects of CO_2 Utilization via Direct Heterogeneous Electrochemical Reduction. *J. Phys. Chem. Lett.* **2010**, *1*, 3451–3458. [CrossRef]
12. Kaneco, S.; Iiba, K.; Katsumata, H.; Suzuki, T.; Ohta, K. Electrochemical reduction of high pressure CO_2 at a Cu electrode in cold methanol. *Electrochim. Acta.* **2006**, *51*, 4880–4885. [CrossRef]
13. Kuhl, K.P.; Cave, E.R.; Abram, D.N.; Jaramillo, T.F. New insights into the electrochemical reduction of carbon dioxide on metallic copper surfaces. *Energy Environ. Sci.* **2012**, *5*, 7050–7059. [CrossRef]
14. Oh, Y.; Vrubel, H.; Guidoux, S.; Hu, X. Electrochemical reduction of CO_2 in organic solvents catalyzed by MoO_2. *Chem. Commun.* **2014**, *50*, 3878–3881. [CrossRef] [PubMed]
15. Chen, Y.; Kanan, M.W. Tin Oxide Dependence of the CO_2 Reduction Efficiency on Tin Electrodes and Enhanced Activity for Tin/Tin Oxide Thin-Film Catalysts. *J. Am. Chem. Soc.* **2012**, *134*, 1986–1989. [CrossRef] [PubMed]
16. Li, C.W.; Kanan, M.W. CO_2 Reduction at Low Overpotential on Cu Electrodes Resulting from the Reduction of Thick Cu_2O Films. *J. Am. Chem. Soc.* **2012**, *134*, 7231–7234. [CrossRef] [PubMed]
17. Dubois, M.R.; Dubois, D.L. Development of Molecular Electrocatalysts for CO_2 Reduction and H_2 Production/Oxidation. *Acc. Chem. Res.* **2009**, *42*, 1974–1982. [CrossRef] [PubMed]
18. Lin, S.; Diercks, C.S.; Zhang, Y.B.; Kornienko, N.; Nichols, E.M.; Zhao, Y.; Paris, A.R.; Kim, D.; Yang, P.; Yaghi, O.M. Covalent organic frameworks comprising cobalt porphyrins for catalytic CO_2 reduction in water. *Science* **2015**, *349*, 1208–1213. [CrossRef] [PubMed]

19. Qiu, Y.L.; Zhong, H.X.; Zhang, T.T.; Xu, W.B.; Li, X.F.; Zhang, H.M. Copper Electrode Fabricated via Pulse Electrodeposition: Toward High Methane Selectivity and Activity for CO_2 Electroreduction. *ACS Catal.* **2017**, *7*, 6302–6310. [CrossRef]
20. Hori, Y.; Takahashi, I.; Koga, O.; Hoshi, N. Electrochemical reduction of carbon dioxide at various series of copper single crystal electrodes. *J. Mol. Catal. A Chem.* **2003**, *199*, 39–47. [CrossRef]
21. Nie, X.; Esopi, M.R.; Janik, M.J.; Asthagiri, A. Selectivity of CO_2 Reduction on Copper Electrodes: The Role of the Kinetics of Elementary Steps. *Angew. Chem. Int. Ed.* **2013**, *52*, 2459–2462. [CrossRef] [PubMed]
22. Sarfraz, S.; Esparza, A.T.G.; Jedidi, A.; Cavallo, L.; Takanabe, K. Cu–Sn Bimetallic Catalyst for Selective Aqueous Electroreduction of CO_2 to CO. *ACS Catal.* **2016**, *6*, 2842–2851. [CrossRef]
23. Shi, G.D.; Yu, L.; Ba, X.; Zhang, X.S.; Zhou, J.Q.; Yu, Y. Copper nanoparticle interspersed MoS_2 nanoflowers with enhanced efficiency for CO_2 electrochemical reduction to fuel. *Dalton Trans.* **2017**, *46*, 10569–10577. [CrossRef] [PubMed]
24. Li, Q.; Fu, J.J.; Zhu, W.L.; Chen, Z.Z.; Shen, B.; Wu, L.H.; Xi, Z.; Wang, T.Y.; Lu, G.; Zhu, J.J.; et al. Tuning Sn-Catalysis for Electrochemical Reduction of CO_2 to CO via the Core/Shell Cu/SnO_2 Structure. *J. Am. Chem. Soc.* **2017**, *139*, 4290–4293. [CrossRef] [PubMed]
25. Ni, M.; Leung, M.K.H.; Leung, D.Y.C.; Sumathy, K. A review and recent developments in photocatalytic water-splitting using TiO_2 for hydrogen production. *Renew. Sust. Energ. Rev.* **2007**, *11*, 401–425. [CrossRef]
26. Liu, G.; Wang, L.; Yang, H.G.; Cheng, H.M.; Lu, G.Q. Titania-based photocatalysts—Crystal growth, doping and heterostructuring. *J. Mater. Chem.* **2010**, *20*, 831–843. [CrossRef]
27. Ravichandran, C.; Kennady, C.J.; Chellammal, S.; Thangavelu, S.; Anantharaman, P.N. Indirect electroreduction of o-nitrophenol to o-aminophenol on titanium dioxide coated titanium electrodes. *J. Appl. Electrochem.* **1991**, *21*, 60–63. [CrossRef]
28. Chu, D.; Qin, G.; Yuan, X.; Xu, M.; Zheng, P.; Lu, J. Fixation of CO_2 by Electrocatalytic Reduction and Electropolymerization in Ionic Liquid-H_2O Solution. *ChemSusChem* **2008**, *1*, 205–209. [CrossRef] [PubMed]
29. Thompson, T.L.; Diwald, O.; Yates, J.T. CO_2 as a Probe for Monitoring the Surface Defects on TiO_2 (110) Temperature-Programmed Desorption. *J. Phys. Chem. B* **2003**, *107*, 11700–11704. [CrossRef]
30. Cueto, L.F.; Hirata, G.A.; Sanchez, E.M. Thin-film TiO_2 electrode surface characterization upon CO_2 reduction processes. *J. Sol-Gel Sci. Technol.* **2006**, *37*, 105–109. [CrossRef]
31. Ma, S.C.; Lan, Y.C.; Perez, G.M.J.; Moniri, S.; Kenis, P.J.A. Silver Supported on Titania as an Active Catalyst for Electrochemical Carbon Dioxide Reduction. *ChemSusChem* **2014**, *7*, 866–874. [CrossRef] [PubMed]
32. Yuan, J.; Liu, L.; Guo, R.R.; Zeng, S.; Wang, H.; Lu, J.X. Electroreduction of CO_2 into Ethanol over an Active Catalyst: Copper Supported on Titania. *Catalysts* **2017**, *7*, 220. [CrossRef]
33. Yuan, J.; Yang, M.P.; Hu, Q.L.; Li, S.M.; Wang, H.; Lu, J.X. Cu/TiO_2 nanoparticles modified nitrogen-doped graphene as a highly efficient catalyst for the selective electroreduction of CO_2 to different alcohols. *J. CO_2 Util.* **2018**, *24*, 334–340. [CrossRef]
34. Fang, B.Z.; Xing, Y.L.; Bonakdarpour, A.; Zhang, S.C.; Wilkinson, D.P. Hierarchical CuO-TiO_2 Hollow Microspheres for Highly Efficient Photodriven Reduction of CO_2 to CH_4. *ACS Sustain. Chem. Eng.* **2015**, *3*, 2381–2388. [CrossRef]
35. Choi, H.J.; Kang, M. Hydrogen production from methanol/water decomposition in a liquid photosystem using the anatase structure of Cu loaded TiO_2. *Int. J. Hydrog. Energy* **2007**, *32*, 3841–3848. [CrossRef]
36. Chi, D.H.; Yang, H.P.; Du, Y.F.; Lv, T.; Sui, G.J.; Wang, H.; Lu, J.X. Morphology-controlled CuO nanoparticles for electroreduction of CO_2 to ethanol. *RSC Adv.* **2014**, *4*, 37329–37332. [CrossRef]
37. Kulkarni, P.; Mahamuni, S.; Chandrachood, M.; Mulla, I.S.; Sinha, A.P.B.; Nigavekar, A.S.; Kulkarni, S.K. Photoelectron spectroscopic studies on a silicon interface with $Bi_2Sr_2CaCu_2BO_{8+\delta}$ high T_c superconductor. *J. Appl. Phys.* **1990**, *67*, 3438–3442. [CrossRef]
38. Ethiraj, A.S.; Kang, D.J. Synthesis and characterization of CuO nanowires by a simple wet chemical method. *Nanoscale Res. Lett.* **2012**, *7*, 70. [CrossRef] [PubMed]
39. Chang, T.Y.; Liang, R.M.; Wu, P.W.; Chen, J.Y.; Hsieh, Y.C. Electrochemical reduction of CO_2 by Cu_2O-catalyzed carbon clothes. *Mater. Lett.* **2009**, *63*, 1001–1003. [CrossRef]
40. Gupta, K.; Bersani, M.; Darr, J.A. Highly efficient electro-reduction of CO_2 to formic acid by nano-copper. *J. Mater. Chem. A* **2016**, *4*, 13786–13794. [CrossRef]

41. Qiao, J.L.; Fan, M.Y.; Fu, Y.S.; Bai, Z.Y.; Ma, C.Y.; Liu, Y.Y.; Zhou, X.D. Highly-active copper oxide/copper electrocatalysts induced from hierarchical copper oxide nanospheres for carbon dioxide reduction reaction. *Electrochim. Acta.* **2015**, *153*, 559–565. [CrossRef]
42. Ghijsen, J.; Tjeng, L.H.; Van-Elp, J.; Esks, H.; Westerink, J.; Sawatzky, C.A.; Czyzyk, M.T. Electronic structure of Cu_2O and CuO. *Phys. Rev. B* **1988**, *38*, 11322–11330. [CrossRef]
43. Mohamed, A.M.; Aljaber, A.S.; AlQaradawi, S.Y.; Allam, N.K. TiO_2 nanotubes with ultrathin walls for enhanced water splitting. *Chem. Commun.* **2015**, *51*, 12617–12620. [CrossRef] [PubMed]
44. Bai, L.; Qiao, S.; Fang, Y.; Tian, J.; Mcleod, J.; Song, Y.; Huang, H.; Liu, Y.; Kang, Z. Third-order nonlinear optical properties of carboxyl group dominant carbon nanodots. *J. Mater. Chem. C* **2016**, *4*, 8490–8495. [CrossRef]
45. Yu, B.Y.; Kwak, S.Y. Carbon quantum dots embedded with mesoporous hematite nanospheres as efficient visible light-active photocatalysts. *J. Mater. Chem.* **2012**, *22*, 8345–8353. [CrossRef]
46. Li, H.; Zhang, X.; MacFarlane, D.R. Carbon Quantum Dots/Cu_2O Heterostructures for Solar-Light-Driven Conversion of CO_2 to Methanol. *Adv. Energy Mater.* **2015**, *5*, 1401077. [CrossRef]
47. Li, C.W.; Ciston, J.; Kanan, M.W. Electroreduction of carbon monoxide to liquid fuel on oxide-derived nanocrystalline copper. *Nature* **2014**, *508*, 504–507. [CrossRef] [PubMed]
48. Wan, Y.; Zhang, Y.; Wang, X.; Wang, Q. Electrochemical formation and reduction of copper oxide nanostructures in alkaline media. *Electrochem. Commun.* **2013**, *36*, 99–102. [CrossRef]
49. Gao, S.; Lin, Y.; Jiao, X.C.; Sun, Y.F.; Luo, Q.Q.; Zhang, W.H.; Li, D.Q.; Yang, J.L.; Xie, Y. Partially oxidized atomic cobalt layers for carbon dioxide electroreduction to liquid fuel. *Nature* **2016**, *529*, 68–82. [CrossRef] [PubMed]
50. Kortlever, R.; Shen, J.; Schouten, K.J.P.; Calle-Vallejo, F.; Koper, M.T.M. Catalysts and Reaction Pathways for the Electrochemical Reduction of Carbon Dioxide. *J. Phys. Chem. Lett.* **2015**, *6*, 4073–4082. [CrossRef] [PubMed]